IOPscience iopscience.iop.org

Home Search Collections Journals About Contact us My IOPscience

Creating pure nanostructures from electron-beam-induced deposition using purification techniques: a technology perspective

This article has been downloaded from IOPscience. Please scroll down to see the full text article.

2009 Nanotechnology 20 372001

(http://iopscience.iop.org/0957-4484/20/37/372001)

View the table of contents for this issue, or go to the journal homepage for more

Download details:
IP Address: 131.180.130.109
The article was downloaded on 08/08/2011 at 09:56

Please note that terms and conditions apply.

Nanotechnology 20 (2009) 372001 (17pp) doi:10.1088/0957-4484/20/37/372001

TOPICAL REVIEW

Creating pure nanostructures from electron-beam-induced deposition using purification techniques: a technology perspective

A Botman[1,3], **J J L Mulders**[2] and **C W Hagen**[1]

[1] Faculty of Applied Sciences, Delft University of Technology, Lorentzweg 1, 2628 CJ Delft, The Netherlands
[2] FEI Electron Optics, Achtseweg Noord 5, 5651 GG Eindhoven, The Netherlands

E-mail: aurelien.botman@fei.com

Received 19 March 2009, in final form 29 June 2009
Published 26 August 2009
Online at stacks.iop.org/Nano/20/372001

Abstract
The creation of functional nanostructures by electron-beam-induced deposition (EBID) is becoming more widespread. The benefits of the technology include fast 'point-and-shoot' creation of three-dimensional nanostructures at predefined locations directly within a scanning electron microscope. One significant drawback to date has been the low purity level of the deposition. This has two independent causes: (1) partial or incomplete decomposition of the precursor molecule and (2) contamination from the residual chamber gas. This frequently limits the functionality of the structure, hence it is desirable to improve the decomposition and prevent the inclusion of contaminants. In this contribution we review and compare for the first time all the techniques specifically aimed at purifying the as-deposited impure EBID structures. Despite incomplete and scattered data, we observe some general trends: application of heat (during or after deposition) is usually beneficial to some extent; working in a favorable residual gas (ultra-high vacuum set-ups or plasma cleaning the chamber) is highly recommended; gas mixing approaches are extremely variable and not always reproducible between research groups; and carbon-free precursors are promising but tend to result in oxygen being the contaminant species rather than carbon. Finally we highlight a few novel approaches.

1. Introduction

The need for the fabrication of ever smaller structures requires, at regular intervals, new types of technologies to be developed [1]. With conventional resist-based lithography in its various forms (light, ultraviolet, x-rays, electrons) approaching its limits [2, 3], research is focusing on novel methods such as self-assembly (bottom-up) and nano-imprint lithography (top-down) to carry out fundamental investigation of the technology at length scales of a few nanometers [4]. One potential technique for such nanometer fabrication, nanoscale rapid prototyping and nanoscale lithography is electron-beam-induced deposition (EBID) [5, 6]. It is a direct-write process where an electron beam locally decomposes a precursor gas. It is used for creating conductive or insulating three-dimensional nanoscale structures within a few minutes inside a scanning electron microscope (SEM) on non-flat substrates. The deposited material depends on the precursor chosen. Capable of producing sub-10 nm structures [7], it finds immediate applicability in the rapidly growing fields of nanoelectronics, data storage, molecular biology and nanofluidics. Typical applications of EBID include nanowire

[3] Present address: FEI Company, 5350 NE Dawson Creek Drive, Hillsboro, OR 97124, USA.

 © 2009 IOP Publishing Ltd Printed in the UK

													C 100%				
												Al ★	Si 100%				
			Ti 35%		Cr ★	Mn ⊗	Fe 100%	Co 97%	Ni 36%	Cu 60%		Ga 50%	Ge 100%				
					Mo 10%		Ru ⊗	Rh 66%	Pd >50%				Sn 58%				
					W 66%		Os ⊗	Ir 33%	Pt 83%	Au 100%			Pb ⊗				

Figure 1. Periodic table of elements for EBID, with best purities obtained. All percentages are at.%, ignoring hydrogen content. ⊗ means no quantitative information on the composition of the deposit is available; ★ means the material is claimed as being 'pure' when deposited, though the claim is not quantitatively substantiated. References in the main text.

deposition [8], contacting carbon nanotubes [9] and growing tips for field emission [10] and atomic and magnetic force microscopy [11]. Best described as an additive lithography process, using direct deposition without the need for resist layers, and having many characteristics in common with chemical vapor deposition (CVD) processes, it has been in use since at least 1976 [12].

Typically the dimensions of the fabricated structure are in the range 20 nm to several μm; with further work, nanowires and nanodots with single-digit nm lateral size can be made [13–15]. Creating those structures with feature sizes below 20 nm is where EBID is especially useful compared to other techniques.

The concept behind EBID is rather simple and can be likened to a very local CVD process: a so-called precursor molecule, containing the material of interest to be deposited such as platinum, gold, copper or tungsten, but still being relatively volatile, is introduced into a vacuum environment (often a scanning electron microscope) in gaseous form in the vicinity of the substrate for deposition. It is adsorbed onto the substrate surface. An electron beam causes dissociation of this precursor by transferring energy to the adsorbed molecules in the vicinity of the beam interaction point. There is considerable evidence that this dissociation is caused principally by the secondary electrons emitted from the substrate [6, 16]. The precursor is dissociated into a volatile and a non-volatile part. The non-volatile part forms the deposit by remaining locally on the substrate, while the volatile fragments leave the area and are eventually pumped out of the system. Typical precursors are $W(CO)_6$ (tungsten hexacarbonyl), Me_2Au(tfac) (dimethyl-gold-trifluoroacetylacetonate) and (hfac)Cu(VTMS) (hexafluoroacetylacetonate-copper-vinyltrimethylsilane).

There now exist precursors for most elements one could wish to deposit. In the following list, a single reference is given for each material (generally the most recent publication known to us); for a more complete cross-reference the reader is referred to one of the many general EBID reviews such as Utke *et al* [17]: Al [18], Au [19], C (abundant literature), Co [20], Cr [21], Cu [22], Fe [23], GaAs [24], Ga [25], Ge [26], Ir [27], Mn [28], Mo [29], Ni [30], Os [31], Pb [32], Pd [33], Pt [34], Rh [35], Ru [31], Si/SiO_x [36], Sn [37], Ti [38] and W [39]. The growth of the deposit can be directed to take the shape of the structure that one wishes to fabricate; indeed such exotic three-dimensional structures as nanobridges can be easily produced (figure 2). Less trivially, EBID has been used to fabricate emitter tips [40, 41] in a manner which would have been impossible to do with any other technique.

Figure 2. An example electron-beam-induced deposited structure: a three-dimensional bridge (platinum material).

Figure 1 shows the periodic table of the elements with each material which can be deposited by EBID as per the previous list; also shown in that figure is the best compositional purity after deposition by EBID reported in the literature for that element.

The values can be found in the following references (this list differs from the first in that the precursors used are not necessarily 'standard'): Al from $Al(CH_3)_3$ [42], Au from $AuCl(PF_3)$ [43], Co from $Co_2(CO)_8$ [44], Cr from $Cr(CO)_6$ [45] with annealing to 330 °C, Cu from Cu-DMB-hfac [22], Fe from $Fe(CO)_5$ in a UHV set-up [46], Ga from

D_2GaN_3 [25], Ge from Ge_2H_6 [26], Ir from $[IrCl(PF_3)_2]_2$ [27], Mn from $MnMeCp(CO)_3$ [28], Mo from $Mo(CO)_6$ [29], Ni from $Ni(PF_3)_4$ [30], Os from $Os_3(CO)_{12}$ [31], Pb from $Pb(CH_3)_4$, Pd from Pd(ac) with annealing to 250 °C [47], Pt from $Pt(PF_3)_4$ [48], Rh from $[RhCl(PF_3)_2]_2$ [49], Ru from $Ru_3(CO)_{12}$ [31], Si from Si_2H_6 [50], Sn from $SnCl_4$ [51], Ti from $Ti(NO_3)_4$ [38] and W from WF_6 [52]. Carbon is given as 100 at.% given that contamination deposition is the most common form of EBID; various groups have deposited pure carbon in various forms (amorphous, diamond, etc) and the literature is too abundant to list here. The concentrations in figure 1 ignore the hydrogen content of deposits, since this is difficult to quantify.

EBID is not yet fully embraced as a nanotechnology solution since it does have a few drawbacks which are critical to applications, one of which is the deposit's purity. In the abundant case of the precursor being a metal–organic compound, large amounts of carbon and other species such as oxygen from the precursor fragments or incomplete precursor dissociation are deposited along with the metal, and the resulting material is often described as a matrix of carbon within which there is a little metal [53]. In most cases residual hydrocarbons originating from the vacuum residual gas, SEM chamber walls or substrate surface are also decomposed resulting in additional carbon and oxygen in the deposit. After deposition the deposited structures are usually brought from vacuum into air; as we shall see below this may also be a significant source of deposit contamination, by oxidation of the deposited metal. Side reactions of precursor fragments may also contribute to foreign elements being incorporated into the deposit.

One common application of EBID being the writing of conductive lines at a position chosen by the SEM operator, for example to create contact electrodes to nanoscale devices, the low purity and conductivity of the material as a result of the co-deposited contaminants is often detrimental to the target application. It is therefore relevant to reduce the structures' resistivity as far as possible, ideally to the level of the bulk metal of the material originally desired. Indeed a main metric of deposition success from a technological perspective is the material's resistivity, which is usually related to the metal content compared to the contaminant content. In lower metal content materials, nonlinear I/V characteristics appear and the conduction mechanism changes. Examples of such conduction mechanisms are percolation, phonon-assisted tunneling or Poole–Frenkel conduction. In highly resistive materials conduction mechanisms are an entire field of research in themselves [33, 53–55]. Another technologically important field for EBID is photomask repair, where the requirement is pure SiO_2 deposition for the 45 nm node. A third motivation for pure EBID material is the creation of ferromagnetic structures—in this case it is of interest to deposit pure iron or cobalt with EBID. This subset of EBID research is a growing and active field and there is currently too little literature on the subject to include any discussion of value here. However, the same basic principles and methodologies apply as for obtaining low resistivity structures.

The difficulty behind using analytical techniques for a greater understanding of the fundamental chemical processes occurring during EBID is well illustrated by a quote from an article by Fairbrother *et al* [56]: 'attempts to exert greater control over EBID and improve the purity of deposits have been hindered by a lack of molecular-level understanding regarding the electron stimulated reactions and chemical transformations that underpin the EBID process. This lack of knowledge is in large part a consequence of the fact that EBID is always performed in the presence of a constant partial pressure of the precursor. Under these equilibrium conditions, the relatively high pressure (ranging from 10^{-6} Torr to a few mTorr) precludes the use of most surface analytical techniques, which are capable of monitoring changes in the chemical bonding and composition of the adsorbate layer during electron beam irradiation. The presence of a significant partial pressure associated with the EBID precursor also limits the ability of mass spectrometry to discern gas phase species evolved during the deposition process'.

Several high-quality general EBID reviews have been published in the recent literature by Randolph [5] in 2006, Furuya [57], Utke [17] and van Dorp [58] in 2008. In contrast to those, this review will be specifically focused on the purification aspect of deposited nanostructures from a practical perspective. We shall attempt to condense technological knowledge and this overview should result in a better appreciation of what the current trends and results are. The scope of this review is strictly limited to the purification of electron-beam-induced deposits, where the normal procedure results in an impure deposit. Furthermore while we shall list every known carbon-free precursor and at least one report of its use, we will not reference every article where such are used—for instance, there are now a large number of publications on WF_6.

Higher purity nanostructures have also been achieved using a related technique called ion-beam-induced deposition (IBID), which is essentially identical to EBID but substituting ions for electrons. Typically, IBID is carried out in focused gallium-based ion beam microscopes (FIB). The deposits tend to be of higher purity due to the combined effects of the larger cross section for dissociation by ions, the higher mass of ions leading to more component splitting per reaction and possible beam-induced local heating. However, with IBID, other problems arise, such as gallium implantation from the ion beam, top surface damage and a worse resolution with larger tails [59]. In this review we are not going to discuss ion-beam-induced deposition (IBID) any further, except as an occasional comparison point where convenient.

No attention will be paid to the growing literature on modeling the EBID process by Monte Carlo simulations [15, 16, 60–64], because currently they do not even attempt to describe the composition of the deposited material. Similarly other reviews go into great depth about the exact mechanism behind the dissociation process, trying to determine the relative importance of direct e-beam stimulated dissociation as opposed to e-beam stimulated desorption or dissociative electron attachment [65, 66]; here we do not discriminate between the individual processes. Rather this review focuses on the eminently practical perspective of a user: given a precursor and operating within given experimental

equipment constraints, how can the user maximize the conductivity or purity of the deposit? We shall, of course, attempt to explain why this or the other method works better or is expected to lead to better results and which are the more promising avenues of research; however, as we shall see this kind of discussion just serves to illustrate how fragmented and incomplete research in EBID really is, and the dire need for some standardized tests to establish equivalency across different systems (such as the 'van Dorp checklist' [58]).

2. Categorization

We may divide all the existing purification methods in the literature into seven categories, and we will treat each one in turn. We refer to *in situ* experiments as being performed in the same SEM or instrument that the deposition was performed in (hence no vacuum break) and *ex situ* experiments as those being performed in different instruments. The categories are: (1) annealing the structures after deposition in vacuum and *in situ*, or deposition onto a heated substrate; (2) varying the deposition parameters, such as beam current, scanning strategies, precursor gas pressure, etc; (3) post-treating the structures after deposition in a different set-up (hence *ex situ* given it takes place outside the SEM chamber); (4) post-treating the structures after deposition within the same SEM chamber (hence *in situ*); (5) introducing a second gas into the chamber during deposition, for the purpose of competitively removing a selected species as and while it is being deposited; (6) the use of carbon-free precursors; and finally (7) working in ultra-high vacuum (UHV) set-ups, or taking extraordinary care in obtaining a very clean environment. Together these seven techniques cover all the published literature on EBID structure purification: however, we shall further widen our scope and in an eighth section (8) we will describe some purification techniques in other related fields, in the hope that these may provide ideas for future pathways of pure material deposition when applied to the field of EBID.

It should be noted in what follows that from each publication we extract only what we consider as the main feature or the point of particular interest—while we may, for instance, report that a specific article reported (for example) an increase of 20 at.% in metal content from vacuum annealing at 500 °C for 10 min, it goes without saying that the original article contains much more extensive information and results, and this review only gives an indication of the type of results obtained therein.

Some items are present in more than one category since these are not mutually exclusive. For completeness in the tables they are usually duplicated in each section: however, their extended description is only present in the more relevant category.

3. Techniques for purification

3.1. Annealing deposits or deposition onto a hot substrate

This section deals with purification by application of heat, either during deposition by performing EBID onto a hot sample, or after deposition (*in situ*) and with or without additional reactive gases. Table 1 summarizes the main work in this area.

Deposition onto a hot substrate is meant to purify the deposits by reducing the residence time of contaminants from vacuum and of carbonaceous fragments after precursor dissociation on the substrate surface, hence preventing their inclusion in the material growth, and proportionally giving more time to the precursor to undergo more complete dissociation before the next layer of precursor growth. It suffers from the concomitant effect that the precursor molecule then also has a lower surface residence time and this results in a lower deposition yield [67]. Furthermore the deposit itself may also be less rigidly bonded to the substrate and the deposition geometry may be less well defined due to diffusion over the substrate surface of the precursor fragments after dissociation. The choice of temperature at which to hold the substrate is therefore given by a compromise between these factors.

Once the EBID structure has been deposited, it is still possible to reduce the relative carbon concentration within the structure by applying an annealing step. Vacuum anneals and anneals in various gases have been tried; those annealing steps taking place in the same SEM chamber are listed here whereas those taking place in a separate chamber are classed as *ex situ* and listed in section 3.3.

Generally speaking it can be seen from table 1 that the application of heat always works to some extent to remove carbon or induce crystallization of the deposit. In the case of Au, Cr, Cu, Re and Pt (from $Pt(PF_3)_4$), application of heat always increases the purity and conductivity of the deposits. On the other hand, for other materials (Fe and W), there is the danger of forming alloys and silicides; and tungsten appears to be particularly susceptible to oxidation. Furthermore the results rarely go all the way to pure metal: impurities always remain. Finally an observation which is made by many in the case of elevated temperatures (>400 °C) is the formation of voids within the deposit or geometrical distortions (shape changes) of the deposit, resulting from the large volume loss of carbon (see, for example, [68]). This is clearly undesirable in the case one is trying to make a functional nanodevice.

Interestingly it appears that platinum deposited from $MePtCpMe_3$ is not affected or purified by application of heat alone; this is confirmed by the authors' own experience up to 150 °C. In section 3.3 we will see that an *ex situ* anneal in 1 atm O_2 does, however, increase the platinum content for depositions from this precursor.

The trend can be summarized by the hypothesis that, at higher substrate temperature, the amount of adsorbed contamination from the residual gas on the substrate is lower. Similarly, the dissociated non-metallic fragments are more easily desorbed from hot surfaces, hence the deposit has a higher metal to contaminant ratio. Furthermore because of the lower sticking factor of the precursor molecules, each already-deposited layer has comparatively more time and exposure to the electron beam such that the dissociation may proceed more fully. Nonetheless carbon appears to be difficult to remove completely simply by annealing. Using heat to promote the dissociation of carbon groups from the metal portion of the

Table 1. Summary of the main work in annealing or substrate heating. 'Hot substrate' indicates the deposition was performed onto a heated substrate; in all other cases the heat is applied after the deposition is finished. Items denoted 'IBID' apply to gallium-ion-beam-induced deposited structures rather than those deposited by electron beam.

Precursor	Without treatment	Conditions of treatment	Results of treatment	Reference
Au(hfac) [IBID]	50 at.% Au, 500–1500 $\mu\Omega$ cm	Hot substrate, 125 °C	80 at.% Au, 7 $\mu\Omega$ cm	[109]
Au(acac)	10–15 at.% Au, 10^8 $\mu\Omega$ cm	Post-anneal in 1 atm O_2, 500 °C	60 at.% Au, 10^7 $\mu\Omega$ cm	[68]
$Me_2Au(acac)$	4–6 at.% Au	Post-anneal in air 30 min, 400 °C	20 at.% Au	[19]
$Me_2Au(tfac)$	15 at.% Au	Hot substrate, 100 °C	24 at.% Au	[10]
$Cr(CO)_6$		Vacuum anneal 1 h, 800 °C	Pure crystalline Cr	[110]
$Cr(CO)_6$		Hot substrate, 280 and 330 °C	141 and 79 $\mu\Omega$ cm	[45]
Cu(hfac)VTMS [IBID]	50–135 $\mu\Omega$ cm, 20 nm Cu islands within carbon matrix (50 at.% Cu)	Hot substrate, 100 °C	2–10 $\mu\Omega$ cm, polycrystalline Cu (islands merged, almost no C) (Note: thermal decomposition temperature of this precursor is 64 °C, see [111])	[112]
Cu(hfac)VTMS [IBID]	50 $\mu\Omega$ cm, 40 at.% Cu	Hot substrate, 100 °C	20 $\mu\Omega$ cm, 60 at.% Cu (Note: thermal decomposition temperature of this precursor is 64 °C, see [111])	[113]
$Fe(CO)_5$	48 at.% Fe	Autocatalytic thermal decomposition (induced by high beam current)	Autocatalytic growth region is 82 at.% Fe	[114]
$Fe(CO)_5$	10^6 $\mu\Omega$ cm	Vacuum anneal 1 h, 600 °C	α-Fe phase, 100 $\mu\Omega$ cm	[115, 116]
$Fe(CO)_5$		Hot substrate, 525 °C	Carbon-free crystalline silicides	[117]
$Fe(CO)_5$		Hot $SrTiO_3$ substrate, >500 °C	No deposition (yield is zero) above 500 °C	[118]
$Fe(CO)_5$		Vacuum anneal (600 °C), followed by Pt coating (by evaporation), followed by vacuum anneal (700 °C)	$FePt_3$ alloy	[119]
$MePtCpMe_3$	10–15 at.%, 10^7 $\mu\Omega$ cm	Post-anneal in 1 atm O_2, 500 °C	70 at.% Pt, 10^4 $\mu\Omega$ cm	[68, 120]
$MePtCpMe_3$	10–15 at.%	Post-anneal in N_2, 300 °C	No effect	[68, 121]
$MePtCpMe_3$	10–15 at.%, 10^6 $\mu\Omega$ cm	Anneal in formic gas (H_2/N_2) 1 h, 500 °C	10^5 $\mu\Omega$ cm	[77]
$MePtCpMe_3$	10–15 at.%	Hot substrate, 150 °C	No change, 10–15 at.%	[122]
$MePtCpMe_3$ [IBID]	680 $\mu\Omega$ cm	Vacuum anneal 10 min, 900 °C	72 $\mu\Omega$ cm, observed Pt diffusion and clustering by BSE signal and EDX	[123]
$MePtCpMe_3$ [IBID]	70–700 $\mu\Omega$ cm, 46 at.% Pt	Hot substrate, 120 °C	No effect on resistivity or Pt content; yield goes to zero	[124]
$Pt(PF_3)_4$	35 at.% Pt, 250–2000 $\mu\Omega$ cm	Post-anneal in air/N_2 mixture, 200 °C	26–500 $\mu\Omega$ cm	[125]
$Pt(PF_3)_4$	15at.% Pt, 57 at.% P	Hot substrate (80 °C) and additional O_2	45 at.% Pt, 29 at.% P	[126]
$Pt(PF_3)_4$	Nanocrystalline Pt	Vacuum post-anneal at 127 °C	Single crystal Pt	[86]
$Re_2(CO)_{10}$		Vacuum anneal 1 h, 800 °C	Pure Re crystalline phase	[110]
$W(CO)_6$		Vacuum anneal 1 h, 800 °C	W_2C and W_3O and pure crystalline W	[110]
$W(CO)_6$	2–4 nm nanocrystalline W in matrix composed of amorphous W, C and O	Vacuum anneal 15 min, 900 °C	Polycrystalline W and WC and WO_2 and WO_3	[127]

precursor may be dependent on how tightly bound the carbon group is to the rest of the precursor molecule: for instance, a CH_3 group would be easier to remove (requiring a substrate less hot) than a CH_2 group. One might imagine, then, that the amount of heat required to purify the deposit will vary according to the precursor, and this is indeed what is observed from the scattered data available shown in table 1.

With heat-based treatments, one fear is that carbides are formed, which are extremely difficult to remove and fairly detrimental to metrics such as resistivity, though it is only expected to be significant for the higher temperature treatments, for instance above 400 °C. A further problem which is occasionally reported is diffusion of the substrate material into the deposit or vice versa. Finally, deformation

Table 2. Summary of the main work studying the effects of varying the deposition parameters, such as beam current, scanning strategies, precursor gas pressure, etc, on the purity or conductivity of the deposit. See note in main text regarding the depositions being performed in the precursor- or electron-limited regime.

Precursor	Without treatment	Conditions of treatment	Results of treatment	Reference
$Me_2Au(tfac)$	3 at.% Au	Higher beam current: 1 nA	10 at.% Au	[73]
$Me_2Au(acac)$	4×10^8 $\mu\Omega$ cm	Higher beam current: from 100 to 900 pA	2×10^4 $\mu\Omega$ cm	[128]
$AuClPF_3$		From single slow speed scan to multiple high speed scans at 1 mm s^{-1} (keeping constant dose)	1000× better conductivity	[80]
hfac-Cu-VTMS	14 at.%	Higher beam current: from 0.1 to 1 nA	30 at.%	[20]
$Co_2(CO)_8$	10^7 $\mu\Omega$ cm	Higher beam current: 10 nA	159 $\mu\Omega$ cm	[11]
$Co_2(CO)_8$	12 at.% Co	High beam current: 3 μA	80 at.% Co	[74]
$Co_2(CO)_8$	83 at.% Co	High beam current: 9.5 nA	97 at.% Co	[44]
$Fe(CO)_5$		Slower deposition rate	'Very large' single α-Fe crystals	[129]
$Fe_3(CO)_{12}$	10^9 $\mu\Omega$ cm	Higher beam current: from 11 pA–232 nA	4×10^4 $\mu\Omega$ cm	[130]
$CpPtMe_3$	5.5×10^6 $\mu\Omega$ cm	Higher beam current: 0.2–0.66 pA	1×10^6 $\mu\Omega$ cm	[73]
$MePtCpMe_3$	10^5 $\mu\Omega$ cm	Vary dwell time	No effect	[77]
$MePtCpMe_3$	10^5 $\mu\Omega$ cm	Vary beam energy	No effect	[77]
$MePtCpMe_3$	9 at.%	From 1 kV, 10 pA to 30 kV, 4 nA	17 at.%	[70]
$MePtCpMe_3$	2 nm polycrystalline Pt	Vary beam defocus	No effect	[78]
$W(CO)_6$	High resistivity	Slow scan, long dwell and loop times	lower resistivity	[71]
$W(CO)_6$		Change gas injection nozzle geometry for higher precursor flux	Improved W content	[131]
$W(CO)_6$		Higher beam energy: 20, 200, 400 kV	Less amorphous, bigger nanocrystals	[132]
WF_6	W_3O	Vary dwell time	98 at.% pure β-W core surrounded by WO_3 layer	[133]
WF_6		ESEM mode and post-irradiation with e-beam	Electron-induced material modification: increasing crystallinity with irradiation time	[134]

of the geometrical shape of the deposit nearly always occurs at the higher temperature anneals.

3.2. Variation of beam parameters or deposition conditions

Variation of the beam parameters (such as beam energy, beam current) or deposition conditions (precursor pressure, beam dwell time, etc) can have an influence on the resulting deposition's purity [69–72]. Besides [69–72] there are no significant systematic studies, i.e. results from the entire range of available beam energies, beam currents, dwell times, etc, of the deposition conditions from a purity or resistivity perspective. Usually these systematic studies focus on other metrics such as growth rate or control of deposit shape (e.g. widths of nanopillar depositions). Nonetheless we list in table 2 those articles where two or more deposition conditions with their influence on the resulting deposit's qualities are reported.

It should be noted here that discussions about the use of higher or lower beam currents are usually of little value if no information about the deposition regime (precursor- or electron-limited) is given, especially considering the wide range of precursor pressures and SEM chamber configurations. Detailed discussions concerning this aspect can be found in van Dorp's review [58] and in Utke's review [17]. Nonetheless, for the present analysis we shall assume that very low beam currents lead to electron-limited depositions whereas very high beam currents of greater than 5 nA are rather more likely to be precursor-limited. We have also reported in [70] that the purity is highly dependent on the current density provided at the dissociation point; hence it is clear that for good results optimal focus and stigmation of the beam should be achieved; unfortunately, readers can only assume that this is the case. This may be a further cause for discrepancies when comparing results.

From table 2 we can see that in nearly each case the metal content increases with the beam current [11, 44, 73, 74]. Higher precursor fluxes also tend to lead to larger nanocrystals or grains being formed. The causes might be due to either of two effects. Firstly, as the beam current is increased, for the same total dose the time during which the deposit is exposed to a given electron flux decreases, which shifts the reaction balance from electron-limited to precursor-limited. Accompanying this, the higher beam current might

dissociate the precursor into more, smaller fragments which would be more easily desorbed and thus the deposit left behind would be inherently richer in metal content. The second potential effect would be beam-induced heating. This would facilitate the desorption of the precursor fragments. Evidence for the importance of the latter is argued by Weber *et al* in [73], where the morphology of nanopillars changes (and the purity increases) the higher up a nanopillar one observes heat conductivity decreasing along the length of a nanopillar; this is a strong indication that for certain precursors (Co [75], Cu [76]) beam-induced heating plays an important role. The interest here is further enhanced by the fact that the thermal decomposition range of the material can be significantly lowered by an autocatalytic effect: Co deposited from $Co_2(CO)_8$ or $Co(CO)_3NO$ [75] causes an autocatalytic lowering of the thermal dissociation temperature of the precursor to a level attainable by beam-induced heating. Thus upwards of a certain pillar height, near-pure cores of Co are obtained. Similar behavior has been observed for $Cr(CO)_6$ and $Fe(CO)_5$ [45]. An extensive discussion of beam-induced heating can be found in [17] and [58].

The situation is more confused for $MeCpPtMe_3$: according to [77] and [78] the dwell time, beam energy and defocus have little effect on resistivity and composition. On the other hand, [70] and [73] both report an improvement based on increasing the beam current. The origin of the discrepancy is not clear; however, let us remark in passing that, depending on whether one is operating in a precursor- or electron-limited regime, the effect of varying the beam parameters will be different.

In principle the precursor-limited deposition regime which is obtained at high beam currents may also be achieved using low precursor pressure and moderate beam currents. However, results in this regime tend not be as good as those performed at higher beam currents and 'standard' precursor pressures. The reasons may be that more carbon is included from the hydrocarbon contamination having more time to diffuse into the deposit from larger distances; more influence proportionally of the residual gas (containing water vapor) having more time to interact with the precursor and the just-deposited surface; and possibly the lack of the beam-induced heating effect discussed above. It is therefore generally found that being in the precursor-limited regime at low beam currents yields worse results than being in the precursor-limited regime at higher beam currents.

The dependence of the material resistivity on the scan speed, dwell and loop times was observed by several people: tungsten from $W(CO)_6$ by Hoyle *et al* [71], by Hiroshima *et al* [79] for WF_6 and by Utke *et al* [35] for Me_2–Au–tfac. The trend differs for the deposition of gold from $AuClPF_3$, reported by Utke *et al* [80], but this can be tentatively explained by the fact that this precursor deposits pure gold grains without any carbon matrix. The normal trend, as seen for $W(CO)_6$ and $Fe(CO)_5$, might be explained by a change from electron- to precursor-limited regime; indeed, due to the finite diffusion time precursor molecules require to reach the deposition location, the dissociation will be more complete and less of the non-conducting fragments will be trapped in the deposit before they can desorb. More explicitly, it might take a certain dose (time) to dissociate a precursor molecule to some extent; continuing irradiation (longer exposure of the same molecule) might lead to a fuller, more complete, dissociation. This 'further' dissociation can only occur if this molecule is not buried under subsequent deposition layers, i.e. if the deposition speed is low. Hence for this fuller dissociation it is advantageous to be in the precursor-gas-limited regime.

3.3. *Ex situ post-treatments*

In this category, the deposited structures are taken out of the SEM chamber where they were deposited, and introduced into a different instrument for further processing with the intent of reducing the carbon content or inducing metal crystallization. See table 3.

The annealing of deposits outside the SEM deposition chamber (as opposed to *in situ*) is therefore covered in this section. It may be seen that, for Au, Pt and W, as in the *in situ* case, heating is clearly beneficial for much the same reasons as already discussed above. The annealing in oxygen at 1 atm in particular appears to yield drastic improvements in the case of platinum deposits; in 10 min the resistivity was reduced from $(2.9 \pm 0.4) \times 10^7$ to $(1.4 \pm 0.2) \times 10^4$ $\mu\Omega$ cm. We may observe that annealing the same size structure in O_2 at the same conditions gives better results for Pt structures than for Au—three orders of magnitude improvement in conductivity rather than one. We could speculate that this is due to the initial configuration of the precursor in that the strength with which each carbon is bound to the rest of the molecule differs for one or for the other. Another explanation may relate to the catalytic properties of platinum which would aid the reaction of carbon with oxygen compared to the case with gold with no catalytic properties. A more extensive study with a wider range of annealing temperatures and annealing times may be beneficial to gain a better understanding.

Nonetheless carbon still appears to be difficult to remove completely simply by annealing. The problems of diffusion of the substrate material into the deposit or vice versa are still present. Finally, deformation of the geometrical shape of the deposit nearly always occurs at the higher temperature anneals, which may exclude the technique from being used on delicate nanostructures with small dimensions.

In different work, Botman *et al* [70] have exposed their platinum deposits to a flux of hydrogen radicals (equivalently termed atomic hydrogen) generated by passing H_2 at 20 mbar into a vacuum at 1 mbar over a hot filament. Radiative heat transport from the filament to the sample limited the 'on time' of the treatment, so for instance having the atomic hydrogen flux flowing for one minute gave a sample heating of 150 °C. To extend the treatment time they introduced a cooling period and repeated the experiment ten times, giving a total treatment time of 10 min. Afterwards the structures were analyzed in cross section in a TEM and it was observed that all surfaces exposed to the atomic hydrogen had a 30 nm deep layer that appeared dense. EDX confirmed this layer was carbon-free and this 30 nm was taken as the effective penetration depth of the atomic hydrogen into the deposit. This method was then

Table 3. Summary of the main work studying the effects of post-treating the structures after deposition in a different set-up.

Precursor	Without treatment	Conditions of treatment	Results of treatment	Reference
Au(acac)	10–15 at.% Au, 10^8 $\mu\Omega$ cm	Post-anneal in 1 atm O_2, 500 °C	60 at.% Au, 10^7 $\mu\Omega$ cm	[68]
$MePtCpMe_3$	10–15 at.%, 10^7 $\mu\Omega$ cm	Post-anneal in 1 atm O_2, 500 °C	70 at.% Pt, 10^4 $\mu\Omega$ cm	[68]
$MePtCpMe_3$	10–15 at.%, 10^7 $\mu\Omega$ cm	Exposed to flux of atomic hydrogen for 10 min, 130 °C	30 nm deep layer of pure carbon-free Pt	[70]
$MePtCpMe_3$	10–15 at.%	Exposed to high energy electrons in a TEM	Fully crystalline Pt nanowire (10 nm wide)	[82]
$Pt(PF_3)_4$	35 at% Pt, 250–2000 $\mu\Omega$ cm	Post-anneal in air/N_2 mixture, 200 °C	26–500 $\mu\Omega$ cm	[125]
WF_6	600 $\mu\Omega$ cm	Anneal in H_2 1 h, 500 °C	'Up to three orders of magnitude better conductance', exact resistivity data not provided	[135]

Table 4. Summary of the main work studying the effects of post-treating the structures after deposition *in situ* in the SEM chamber, after the deposition. Items denoted 'IBID' apply to ion-beam-induced deposited structures rather than those deposited by electron beam.

Precursor	Without treatment	Conditions of treatment	Results of treatment	Reference
$Cu(hfac)_2$	11 at.% Cu	H microplasma 60 min	21 at.% Cu	[81, 136]
$MePtCpMe_3$	10^6 $\mu\Omega$ cm	Implantation of Ga ions to match IBID content (see main text)	10^5 $\mu\Omega$ cm	[77]
$MePtCpMe_3$ [IBID]	20 at.% Pt, 600 $\mu\Omega$ cm	Current-induced self-purification	Slight increase in resistivity; formation of $PtGa_2$	[137, 138]
$Pt(PF_3)_4$	Amorphous	Post-irradiation with e-beam	Crystalline	[86]
$W(CO)_6$ [IBID]	75 at.% W, 300 $\mu\Omega$ cm	Current-induced self-purification	55 $\mu\Omega$ cm	[137, 138]
$W(CO)_6$		Post-irradiation with 1 MeV electrons	Crystalline W	[85, 88]
WF_6		ESEM mode and post-irradiation with e-beam	Electron-induced material modification: increasing crystallinity with irradiation time	[134]

extended by Miyazoe *et al* [81] to the *in situ* case, and this is discussed in section 3.4 below.

Irradiating deposits with an electron beam is normally performed in the same set-up as the original deposition and hence most of the work in this category is classed in the *in situ* section below; Gazzadi *et al* [82] have post-irradiated their deposits with high energy electrons in a TEM (making this an *ex situ* post-treatment). They have observed that this led to their 10 nm wide nanowires to become fully crystalline. For structures of this dimension, we can only assume the principal mechanism would be beam-induced heating leading to self-rearrangement of atoms to a lower energy configuration and hence single crystals. Furthermore we point out that carbon is sufficiently light to be sputtered by the impact of electrons with energy higher than 80 kV [83].

3.4. *In situ* post-treatments

Usually for reasons of simplicity, if one wishes to apply a post-treatment on a deposit, it is preferred to post-treat the deposits in the same SEM chamber as they were deposited in. This has the additional advantage that the deposits are then not exposed to air prior to their purification, which may prevent adverse processes such as water-vapor-induced oxidation that some have observed. One attempt at the quantification of this may be found in [84].

The *in situ* post-treatment experiments are grouped in table 4. Excluded from discussion here are the *in situ* annealing procedures as they are already listed in section 3.1.

The *ex situ* atomic hydrogen post-treatment discussed in section 3.3 was replicated by Miyazoe *et al* [81] who generated a hydrogen microplasma *in situ* confined to a small volume around the deposition target area. The precursor material in this instance was $Cu(hfac)_2$ and the treatment improved the concentration from 11 to 21 at.% over the entire volume of the deposit. Of note is the fact that much longer treatment times (around an hour) were necessary to obtain this result, compared to the *ex situ* treatment described above. Unfortunately no cross section had yet been performed of the treated deposit so it was not possible to tell whether a 'penetration depth' effect was also seen. Using the microplasma simultaneously to deposition was not yet possible due to the RF interference from the plasma generator.

Langford *et al* [77] tried to determine why the IBID deposits were better than the EBID deposits for the same precursor, more specifically whether the better conductivity was a result of the gallium present in the IBID deposits, since the beam used in the IBID depositions was gallium which resulted in Ga implantation. Therefore they deposited a structure with EBID and subsequently irradiated the deposit at low dose with the ion beam, also present on the same machine, thereby implanting gallium in the EBID deposit to the same concentration as found in the IBID deposit. One order of magnitude improvement was obtained, but the resulting resistivity was still high compared to IBID deposits. Hence it can be safely assumed that the gallium alone is not responsible for the better conductivity of IBID deposits, and

the improvement observed in the experiment may simply be due to beam-induced heating from the exposure to the ion beam or to preferential sputtering of carbon atoms due to their lower mass.

Current-induced purification is an interesting concept. Starting out with the high resistivity deposits, a moderately high current is passed through the deposit, the magnitude of which is below the electromigration and failure thresholds, but sufficiently high to induce so much self-heating of the wire that conductivity improves. Thus a local vacuum post-anneal effectively takes place and we may see that this process is effective for IBID-deposited tungsten from tungsten hexacarbonyl but not for the platinum organometallic precursor. The latter may be linked to the failure of improvement also on hot substrates; it could be the case that a sufficiently high temperature is simply not reached for effective carbon loss from this material.

Xie *et al* [85] repeated the same experiment as Gazzadi *et al* [82] in section 3.3 of post-irradiating the deposits with electrons, but with a different precursor and in the same deposition chamber, and found essentially a similar result: the metal (tungsten in this case) had become polycrystalline. Post-irradiation also successfully transformed amorphous $Pt(PF_3)_4$ depositions into crystalline ones ([86]). From Monte Carlo simulations Randolph *et al* [67] found that tips can undergo a temperature rise of up to 50 °C, depending on the primary beam energy and tip height. Though it is difficult to exactly measure such a local temperature increase directly, beam-heating effects would be consistent with many features of EBID deposits observed in the literature. Such a large heating effect effectively changes the dissociation pathway and may also change the morphology of the already-deposited material. If the thermal decomposition temperature is within reach of the beam-induced heating then thermal dissociation will occur in parallel to direct electron-beam-induced dissociation, and the former will inherently give higher purity deposits due to the fact that the precursor is more fully dissociated, giving smaller and more fragments which are hence more volatile. This effect is enhanced for precursors where the metal has an autocatalytic effect (such as Co, discussed above) and absent for those where the thermal dissociation temperature is extremely high (such as TEOS).

In a conflicting experiment, Hoyle *et al* have shown [87] for $W(CO)_6$ that once the initial growth of material has taken place such that there is a continuous wire rather than discrete nuclei of material, the conductivity increases linearly with the wire thickness. This implies that, in this case, the material on the bottom of the wire is not affected by growth of material on top or by the influence of the electron beam in a post-irradiation manner. This is in contrast to other results for the same precursor [85, 88] where a post-irradiation at 1 MeV had a clear effect on the overall resistivity. It might be argued though that the energies dumped into the deposit were significantly different due to the geometries and materials chosen, such that in the latter case far more beam-induced heating was achieved. Thus it might be the case that Hoyle *et al* were simply below the energy threshold required to have any purification effect. Another possible explanation could be that the extremely high energy beam physically knocks carbon atoms out (light element selective milling). This interpretation is substantiated by Egerton *et al* [83].

We can summarize the effect of extra exposure by the electron beam as follows: (1) more complete dissociation, or rather a second dissociation step, of the already-deposited material, (2) beam-induced heating, (3) carbon graphitization, rendering those areas (and hence the overall deposit) more conductive, and more speculatively (4) the formation of volatile fragments by beam-induced reaction with the residual gas. The latter claim might be substantiated by pointing out the residual gas is mainly composed of water vapor, and at higher water vapor concentrations (so-called environmental mode, ESEM) the water vapor is capable of etching and removing carbon on the substrate in a beam-induced reaction [89].

Other results not mentioned in table 4 are, for instance, those of Weber *et al* [73] who found that the metal content of tips increased with decreasing beam energy for various precursors—however, quantitative information is not given. Others (such as Folch *et al* [90]) found no such effect for the same precursor (Me_2–Au–hfac), so the situation is unclear. One possible explanation would be that, due to different deposition geometries (such as pillars in one case and flat squares in the other), the amount of beam-induced heating is different and hence the experimental situation is no longer identical. This further demonstrates the importance of listing every detail of the deposition conditions, as otherwise it is nearly impossible to properly compare results and repeat the experiments.

3.5. Reactive gas mixing

For EBID performed in the high vacuum (HV) SEMs, the precursor is not the only gaseous species present. Indeed the residual gas at 10^{-6} mbar is composed mainly of water vapor, nitrogen, oxygen and small amounts of hydrocarbon contaminants. These influence the properties of the deposit in that they are competing for adsorption sites on the surface with precursor molecules. They then get incorporated into the deposit or react with the precursor in a beam-induced reaction to form oxides, carbides or other undesired entities which also get incorporated into the deposit. In both cases the result is usually detrimental to the deposit's composition and conductivity. Oxides and insulating materials are not always undesirable, however, and a comprehensive list of experiments giving pure UV transparent dielectrics and metal oxides can be found in [17].

Despite the apparent advantage in performing EBID in better vacuum systems, some research has investigated the opposite case, where the background gas level was significantly raised so as to be comparable to or exceed the pressure of the precursor gas. The hope being that the background gas, now termed reactive gas, would selectively react with one of the precursor fragments or somehow be active in the dissociation process such that the material remaining on the surface is of a higher purity. Alternatively the already dissociated unwanted fragments would be made more volatile by the reaction with the reactive gas. The relevant work in

Table 5. Summary of the main work studying the effects of introducing a second gas into the chamber during deposition, for the purpose of competitively removing one species as and while it is being deposited. Items denoted 'IBID' apply to ion-beam-induced deposited structures rather than those deposited by electron beam.

Precursor	Without treatment	Conditions of treatment	Results of treatment	Reference
Au(acac)		Mix H_2O (ESEM, 1.2 mbar)	Solid gold core	[139]
Au(hfac)	25 at.% Au	Mixing Ar/O_2 (13 mbar)	50 at.% Au	[90, 140]
Me_2Au(acac)	4–6 at.% Au	Mix H_2O at 1 mbar	3–5 at.% Au	[19]
$Fe(CO)_5$	50 at.% Fe	Mix H_2O in 1.5:1 ratio	Carbon-free crystalline Fe_3O_4	[141–143]
$Ni(PF_3)_4$ and $Ni(C_5H_4CH_3)_2$	40 and 10 at.% Ni	Mix 1 sccm O_2	Additional O in deposit	[30]
$Ni(PF_3)_4$ and $Ni(C_5H_4CH_3)_2$	40 and 10 at.% Ni	Mix 1 sccm H_2	Tripled H_2O background level and resulted in additional O in deposit	[30]
$MePtCpMe_3$ [IBID]	46 at.% Pt, 70–700 $\mu\Omega$ cm	Mix H_2	No effect	[124]
Me_3PtCp		Mix H_2O	No effect	[144]
$MePtCpMe_3$	10–15 at.% Pt	Mix H_2O at 8×10^{-6} mbar	50 at.% Pt	[145]
$Pt(PF_3)_4$	15 at.% Pt, 57 at.% P, 5 at.% O	Hot substrate (80 °C) and additional O_2 (0.8:1 ratio)	45 at.% Pt, 29 at.% P 25 at.% O	[126]
Siloxane	6 at.% C	Mix O_2 in 3:1 ratio	0 at.% C	[146]
Organosilicanes		Mix 1 sccm O_2	Additional O in deposit at expense of C	[147]
Organosilicanes	15 at.% C	Mix O_2 (amount not given)	0 at.% C	[148]
$W(CO)_6$		Mix H_2O in 4:1 ratio	Little effect on C content; carbon-rich WO_3	[143]
WCl_6		Mix with H_2	58 at.%	[52]

this category is listed in table 5. The simplest example might be Matsui *et al* [52] who mixed H_2 with the WCl_6 precursor in the hope of forming HCl and hence reducing the inclusion of Cl in the deposit. The attempt was described as 'successful': the amount of tungsten was increased from an unspecified amount to 58 at.%.

Besides this, the only recent attempt (Perentes *et al* [30]) at mixing H_2 and EBID (the idea being to react with C from the dissociated fragments and form volatile CH_4) resulted in an interesting observation: when H_2 was introduced in the SEM chamber, the background (residual gas) level of H_2O was tripled (as measured by a residual gas analyzer). One could presume that there is a competition between H_2O and H_2 for adsorption sites on all surfaces in the SEM, and this experiment suggests that H_2 wins. It would be interesting to repeat this experiment in a chamber where the residual water vapor concentration is low to begin with, such as in a UHV set-up. In the case of IBID, the only experiment was with $MePtCpMe_3$ and no effect was observed.

Usually the principal reactive gases used are O_2 and H_2O, the target species being carbon. The hope was that the H_2O or O_2 would react (possibly induced by the electron beam) with the carbon from the deposit to form CO or CO_2. However, as we have observed [84] the residual water vapor is capable of oxidizing platinum, or at the very least to increase the resistivity of the deposits, so this technique would presumably only be effective when one is trying to deposit noble metals. Despite this, oxidation or at least oxygen inclusion is occasionally seen as a worthwhile tradeoff for a lower carbon content. Thus we see in table 5 that in the case of Fe, Ni, Pt and W an increase of O was always seen. Only for gold does there not seem to be an increase; notably, gold is also non-oxidizable.

The actual results for the other metals vary widely. In the case of O_2 mixing on silicon depositions, the small amount of carbon present initially is removed completely. O_2 mixing with $Pt(PF_3)_4$ improved the platinum to phosphorus ratio but overall resulted in less metal content due to the increased oxygen. Additional oxygen was also seen in Ni deposits after O_2 mixing but no change in the relative amount of Ni; the loss of carbon was exactly compensated by the gain of oxygen.

Mixing water vapor seems to be very dependent on the set-up, precursors and pressures used. Solid gold cores were obtained in ESEM mode for Au(acac) but for Me_2Au(acac), an almost identical precursor with identical partial pressure of water, almost no effect was seen. Iron is oxidized to Fe_3O_4 with full carbon loss, whilst tungsten is oxidized to WO_3 with no effect on carbon concentrations. Platinum is substantially improved from 11 to 50 at.% Pt but this seems to be at odds with our recent results on oxidation of deposits over time exposed to water vapor in air [84]. In this area more than any other, the results of almost identical experiments are clearly contradictory; systematic and repeated experiments would clearly be beneficial. This is due in no small part to the difficulty in standard SEM systems of quantifying the exact composition and amount of residual/background gas.

3.6. Carbon-free precursors

To prevent carbon from being contained in the EBID structure it is clear that a carbon-free precursor should be used. To date the choice of such precursors has been poor due to the required combination of material properties. The material's vapor pressure must lie within a usable range. The relevant metal atom to be deposited must be weakly bonded to the carrier part of the precursor molecule so that dissociation can occur under

Table 6. Summary of the main work studying the effects of using a carbon-free precursor.

Precursor	Results	Reference
$AlCl_3$	No Al, only C	[18]
$AuCl(PF_3)$	Percolating pure gold grains, 22–43 $\mu\Omega$ cm	[9, 43]
D_2GaN_3	GaN	[25]
Ge_2H_6	Pure Ge	[26]
$[IrCl(PF_3)_2]_2$	33 at.% Ir	[17, 27]
$Ni(PF_3)_4$	36 at.% Ni, 10^3 $\mu\Omega$ cm	[30]
$Pt(PF_3)_4$	30–650 $\mu\Omega$ cm, up to 81 at.% Pt	[48] amongst others
$[RhCl(PF_3)_2]_2$	60 at.% Rh	[43, 92]
Si_2H_6, SiH_4	Amorphous Si with H embedded; annealing releases H and forms crystalline Si	[50, 149]
$SnCl_2$, $SnCl_4$	58 at.% Sn, 290 $\mu\Omega$ cm	[51, 150]
$TiCl_4$	Composition of $TiCl_x$ film not given	[151]
$Ti(NO_3)_4$	35 at.% Ti, 8 at.% N, 58 at.% O	[38]
WCl_6	58 at.% W	[52]
WF_6	β-W clusters	[91] amongst others

electron irradiation, but not too weakly such that dissociation occurs spontaneously. The material should not decompose over reasonable timescales, so the shelf lifetime should be greater than a few months at typical ambient conditions, and it should not be adversely affected by exposure to water vapor (air moisture), for example. The material should be chemically compatible with the other materials present in the SEM, storage and injection systems. Finally it should not be unduly toxic to humans. As a result of these general selection criteria, good carbon-free precursors are difficult to find. All the discovered ones to date contain chlorine or fluorine, which are capable of beam-induced etching reactions as well as having a negative impact on the deposition chamber itself. Furthermore these compounds also tend to be more toxic to humans than their carbonaceous counterparts; hence specialized equipment is necessary to ensure the safety of the SEM operators. The destruction of SEM equipment and human toxicity are the principal reasons for the general non-adoption of promising carbon-free precursors such as WF_6.

Table 6 gives an overview of those that have been experimented with to date; we have listed each known carbon-free EBID precursor but not necessarily every publication where its use is reported.

Of particular interest is $AuClPF_3$ (chloro-gold-trifluoro-phosphine) which gives pure gold deposits, apparently reproducibly. Unfortunately this precursor suffers from the double drawback that it is difficult and expensive to produce and indeed is not commercially available, and that it decomposes within a few hours in contact with metal at room temperature (it does have a shelf life of a few months if stored in a glass container at $-20\,^{\circ}C$). It is therefore incompatible with most commercial gas injection systems. As a result it has only been used in one group at EPFL [9, 43]. It is very likely that its almost-spontaneous decomposition property makes it such a good EBID precursor.

WF_6 is an aggressive precursor which is known to damage the SEM equipment; presumably the fluorine reacts with water vapor to form HF which is then destructive to many materials present in the SEM chamber. Despite this, deposition from WF_6 is reported by Matsui *et al* [91] and by many others. In [91] the deposition was performed at 5×10^{-8} mbar and there is no mention of oxidized tungsten (W_3O or WO_3)—the article leads us to believe the deposit is pure beta-phase tungsten. Other reports of depositions performed at more standard background pressures of 10^{-6}–10^{-5} mbar vary in the amounts of pure tungsten compared to oxidized tungsten (amorphous or crystalline). We have not seen a clear dependence on reported experimental conditions to date, but the trend does appear to be that the amount of oxide in the deposit correlates with the background chamber pressure (and hence, residual water vapor). It is therefore the authors' present belief that the amount of residual water vapor in the residual gas of the SEM chamber during deposition which, together with electron dose and precursor flux, determines the oxidation level.

The present authors have a demonstration of the importance of oxygen non-inclusion: in the course of our work with $Pt(PF_3)_4$, a carbon-free precursor, an experimental set-up glitch resulted in additional oxygen being included in some deposits done in an otherwise identical manner to others. EDS and resistivity data are available for both; deposits with 15 and 59 at.% oxygen (but otherwise identical) had resistivities of 573 $\mu\Omega$ cm and 2×10^7 $\mu\Omega$ cm, respectively. Clearly, the former value is more desirable than the latter and close attention should be paid to the amount of oxygen being incorporated into deposits. Until now, not much attention to this aspect is seen in the literature. Some authors are, however, starting to include residual gas pressures in their reporting, see, for example, [17].

Deposition of Rh from $[RhCl(PF_3)_2]_2$ gave depositions containing 60 at.% Rh. It is curious, then, that with the carbon-containing precursor $[RhCl(CO)_2]_2$ the purity should not be dramatically decreased: it is still around 55 at.% [92]. This work is particularly interesting because we obtain confirmation of several items: (1) PF3 is not released as one entity but in fact each F is successively removed from the P before the P is removed; (2) the concentration of Rh and Cl is equal; (3) O is present at 8 at.% in the carbon-free version whereas it is only just detectable at 2 at.% in the carbonaceous version. The latter seems to confirm that PF3-based precursors have a propensity to include oxygen in the deposits. The most likely mechanism would be a reaction of PF_3 with residual H_2O to form various amounts of HF, OH and any of PH_3, H_3PO_4, P_2O_5, P_4O_6 or H_3PO_3—in any case the oxygen would subsequently be incorporated into the deposit.

For PF_3-based precursors, it is often found that electrons induce the breaking of the P–F bond rather than the complete removal of the PF group as one would expect from thermal considerations and CVD experience. This difference in decomposition indicates a different mechanism is at work and that full electron-induced dissociation is not simply a single-step process.

Further observations: fluorine is almost never found in the deposited material. Phosphorus has been observed to cluster

Table 7. Summary of the main work studying the effects of working in ultra-high vacuum (UHV) set-ups, or taking extraordinary care in obtaining a low residual gas pressure.

Precursor	Without treatment	Conditions of treatment	Results of treatment	Reference
$Fe(CO)_5$		UHV set-up, low energy beam (2 kV)	Pure Fe	[23, 152]
$Fe(CO)_5$		UHV set-up	95 at.% Fe	[46]
WF_6	Non-reproducibility, 600 $\mu\Omega$ cm	Prior to deposition, O_2 plasma clean for 10 min and 300 °C anneal for 1 h	Reproducible, 300 $\mu\Omega$ cm	[153]
WF_6		O_2 plasma clean prior to deposition	5 s: improves conductivity; 60 s: no improvement	[135]
WF_6		Broad e-beam, UHV set-up, sample cooled to 77 K	Pure W	[154]
XeF_2	Instead of expected beam-induced etching, only beam-induced carbon contamination growth was seen (Si substrate)	Air plasma clean using Evactron [93]	Etching into Si substrate	[155]

in deposits in some cases and then to evaporate under intense electron beam irradiation [84].

3.7. UHV set-ups or working clean

The importance of obtaining a low content of water vapor and hydrocarbons in the residual gas is of critical importance once the deposition regime is such that the deposition rate is low enough that these contaminants form a large part of the final deposit composition. Moreover, if the conductivity of the deposit is sufficiently far from the metallic range due to the high level of carbon and low connectivity of metal content (given the small size of the metal grains and a simple surface to volume ratio interpretation), even slight variations in the amount of water vapor locally at the deposition site will cause varying levels of metal oxidation, provided it is susceptible to being so oxidized. This significantly impacts the resulting conductivity [84]. An obvious way to achieve a lower residual gas level near the deposit is by having better vacuum conditions, therefore going to ultra-high vacuum (UHV) which is usually defined to be better than 10^{-9} mbar. The time it takes for one atomic layer of gas to adsorb on a surface in vacuum is known as the monolayer formation time; for 10^{-6} mbar, it is of the order of magnitude of 1 s (depending on sticking coefficient, surface type, etc) whereas at 10^{-9} mbar, it is of the order of 1 h. Therefore in normal EBID depositions the precursor is competing for adsorption sites with (mainly) water vapor, whereas in UHV depositions the deposition is usually finished before significant water vapor has accumulated. Hence (see table 7) less oxygen is observed in the deposits and reproducibility is increased.

UHV set-ups not only help to reduce the amount of oxygen in the deposit, but as shown by groups in Japan [23] and more recently by Lukasczyk *et al* [46], when used in conjunction with the $Fe(CO)_5$ precursor, no carbon is found in the deposit despite the organometallic nature of the precursor. The mechanism behind this process is still poorly understood; it may be that the residence time of the precursor is enormously increased by the lack of the usual competitive water vapor adsorption on the substrate, and this allows the dissociation process to complete fully (all five carbonyl groups) before the subsequent precursor layer is adsorbed and decomposed.

It has also been suggested [56] that the improved purity may somehow be due to a change in the binding energy of the deposits to the surface under clean substrate conditions (inherently necessary in UHV) compared to contaminant-terminated substrates. It is currently unclear what role this may play in the precursor dissociation process.

If a UHV set-up is not available then simple steps such as baking the sample and plasma cleaning the chamber (for instance with the Evactron decontaminator [93]) help enormously already [70]. In all reported cases, the Evactron plasma cleaner is effective for removing hydrocarbons.

3.8. Other precursors

In the previous sections we have discussed various purification techniques and in section 3.6 we discussed carbon-free precursors. To provide a complete picture of the state of the art, in this section we discuss precursors which, despite being carbon-containing and despite having had no extra purification process, seem to provide high purity deposits. See table 8.

Tetrakis isobutyl diaurum difluoride, $(C_4H_9)_4Au_2F_2$, also appears to give excellent results, according to a single paper from 1995 [94]. Bulk resistivity of gold is mentioned and so is the fact that the core is solid gold; few other quantitative details are given besides chemical bond excitation energies. The other two precursors in the same paper, bis isobutyl aurum (III) cyclohexyl palladium (II) difluoride and dicyclohexyl dipalladium difluoride, are only stated to yield a 'solid metal core' with few quantitative details.

Anecdotally the vinyl-trimethyl-silane (VTMS) variants of copper precursors have been known for some time to produce good copper depositions in the sense of low resistivity, and this is confirmed by [95] as 3.6 $\mu\Omega$ cm; this is very surprising given the still high carbon content (only 10 at.% Cu). The authors themselves admit there is a discrepancy here but give no satisfying explanation or

Table 8. Summary of reported uses of carbon-containing precursors nonetheless giving high purity depositions.

Precursor	Results	Reference
Tetrakis isobutyl diaurum difluoride $(C_4H_9)_4Au_2F_2$	2.4 $\mu\Omega$ cm (i.e. bulk Au resistivity)	[94]
Bis isobutyl aurum (III) cyclohexyl palladium (II) difluoride $(C_4H_9)_2AuF_2Pd(C_6H_{11})$	Solid metal core (few concrete details)	[94]
Dicyclohexyl dipalladium difluoride $[FPd(C_6H_{11})]_2$	Solid Pd core (few concrete details)	[94]

hypothesis. Interestingly when one peruses the rest of the literature on this precursor [20, 27, 49, 96–99], the resistivity measurement has apparently only been repeated once, by Luisier *et al* [22]. They found that the material (containing 20 at.% Cu) was electrically insulating, a finding which questions the results obtained in [95].

3.9. Related techniques

In this section we look at a few techniques that are used in nanofabrication processes being related to increasing purity of deposits, but which are not currently applied or even applicable to EBID. Rather, they are presented here because they might stimulate further ideas on purification of EBID structures and lead to insight as what techniques are most likely to work. See table 9.

There is a large body of literature on CVD. For platinum deposition from CVD, the precursor $MePtCpMe_3$ is often used and leads to pure platinum films. This fact alone suggests that the dissociation pathways behind CVD and EBID are fundamentally different and hence techniques which are applicable in one area are likely not relevant in the other. One reference to a comprehensive review of platinum deposition from CVD is nonetheless provided [100] for the interested reader; the effects of mixing of H_2, O_2 and other gases are covered therein.

The emerging technique of atomic layer deposition (ALD) is of interest because it too is capable of producing pure platinum films from the same precursors [101]. It differs from CVD in the sense that greater control over height growth can be achieved, right up to the monolayer level. However, to date the technique, like CVD, is not local; only large-area thin film growth is possible.

In general, what we can observe is that heat treatments in the form of annealing, post-baking, hot substrates are often successful in reducing carbon from carbon-containing films and structures. There is confirmation that oxygen-rich atmospheres will produce oxides even in CVD [102] and that the resistivity of the films are a strong function of the degree of oxidized material [103].

Two examples of atomic hydrogen use were found in EBID-related fields. The first is in [104] where the authors used atomic hydrogen combined with heat for substrate cleaning; a clean substrate is critical for the subsequent processing. They were able to confirm that it is the hydrogen radicals which were most responsible for the hydrocarbon removal, by demonstrating that simply heating or H_2 fluxes alone did not achieve the desired effect.

The second example is perhaps more striking and relevant. Instead of using an electron or an ion beam to dissociate the precursor locally as in EBID or IBID, Chiang *et al* [105] used directly an atomic hydrogen beam (thermal energy). They were not able to use a focused beam, but they were able to show that where the substrate had been exposed to the beam in the presence of the hfac-Cu-VTMS precursor, near-pure copper deposits were obtained containing 99 at.% Cu and having a resistivity of only 5 $\mu\Omega$ cm. A range of energies were present in the hydrogen beam, from thermal to 500 eV—the species were not actively extracted from plasma so the energies were given by the species velocity and the plasma temperature.

Basu *et al* [106] developed an interesting twist on the EBID method. They used the electron beam on an insulating substrate to generate a charge landscape. Nearby on the same surface, they heat some solid gold to 1045 °C, which is just below the melting point. They found that 'gold vapor' then deposits at points on the surface where charge buildups were present. They claim that the deposited nanostructures are pure metal and that the feature resolution limitation is no longer given by the beam profile but rather by the specific charge landscape obtained. They demonstrate features as small as 20 nm.

4. Conclusions

In this review we have listed and compared all the techniques published in the literature to date which were specifically aimed at purifying the normally impure EBID structures. We have outlined seven main approaches and presented to the reader the most recent results for each. We have shown that the main pathways for improvement in common use today are heating (during or after deposition) and working in a favorable residual gas (UHV set-ups or plasma cleaning the SEM chamber). Results from reactive gas mixing are extremely variable and not always reproducible between research groups. Using a carbon-free precursor in the first instance is also a favorable approach: however, then the contaminant element becomes oxygen rather than carbon, resulting in oxides of the metal being deposited, fatally increasing the resistivity of the structures. The most promising pathway currently observed is the treatment with atomic hydrogen, although significantly more work needs to be performed in this area.

As a general comment, despite potentially being critical, almost no attention is paid to the state of the residual gas during, before or after deposition. This is inherent in the fact that the experiments are carried out in non-UHV conditions: however, this results in an undefined condition of the substrate surface. This lack of knowledge is now clearly problematic when attempting to create pure nanoscale structures. Utke's review [17] goes further than most in the full reporting of parameters. Another parameter often overlooked in the literature is the precursor molecule flux impinging on the substrate at the point of EBID processing. This rapidly renders

Table 9. Summary of selected purification techniques in other, related fields.

Technique/field	Results	Reference
Atomic layer deposition (ALD) of $MePtCpMe_3$ at 300 °C with 40 sccm of O_2	Carbon-and oxygen-free Pt, 12 $\mu\Omega$ cm	[101]
Spin-coated film of palladium hexadecylthiolate, post-heated to 230 °C	Post-heating removed C from film completely	[156]
Atomic H beam (non-focused) to dissociate Cu(hfac)VTMS onto substrate	99 at.% Cu and 5 $\mu\Omega$ cm	[105]
Charged landscape deposition with nearby reservoir of gold at 1045 °C	Pure Au nanodots	[106]
UV decomposition of polymeric Au mercaptone with 250 °C post-bake	Pure Au	[157]
MOCVD of Pt(hfac) with O_2 mixed in	PtO_2 film	[102]
Pt sputter-deposited thin films	Small changes in PtO_2 stoichiometry result in large changes in resistivity	[103]
MBE of GaAs with atomic hydrogen flux (from hot filament) for cleaning for 1 min at 700 °C and 8×10^{-6} mbar	Clean substrate and low dislocation density; just heating or just H_2 flow had no effect	[104]
CVD of Pt(acac) with added CO_2	No effect	[158]
CVD of Pt(acac) with post-anneal at 550 °C in O_2	Carbon-free film	[158]
CVD of $Pt(CO)_2Cl_2$	Carbon-free film	[158]

work from different groups non-comparable. How the gas flux can be quantified at the EBID position is comprehensively discussed in a recent article by Friedli *et al* [107].

Furthermore, EBID is a delicate interplay between various factors, and what we are trying to do as researchers is to selectively tweak one or more of these in a serial, repeatable manner. That they are interdependent, and that we cannot actually exert control over each of them, is what renders this research so challenging. A good starting place would be the correct and extended reporting of the full deposition conditions including molecular fluxes of each species present, pressure ranges and residual gas levels (for example, H_2O partial pressures). For this we recommend the use of the 'van Dorp checklist' [58] as a good starting point.

If one were to speculate as to how, given the knowledge available today and reviewed above, one would have the highest chance of creating high purity structures from EBID, one might proceed using a combination of techniques along the lines of figure 3. One should clearly start with an appropriate precursor chemistry, where the precursor molecule is stable enough for transport and handling, but unstable enough such that the electron beam provides sufficient energy to fully dissociate the entire molecule. Use of the appropriate beam energy, current, dwell times and so forth with the aim of providing the highest energy transfer to the molecule to provide a clean and rapid dissociation is subsequently equally desirable. Further, depositing on an already hot substrate minimizes the amount of additional hydrocarbon contamination diffusing into the deposit during growth. Working in a residual gas containing few detrimental contaminants such as hydrocarbons, water and oxygen is by now reasonably obvious, though this in essence requires a UHV-type set-up which may not be practical for common EBID. Finally, post-irradiating the deposits with the electron beam, which essentially continues to dump energy into the structure such that grain formation processes may occur, is beneficial. Given a combination of the these techniques, one may hope to produce 'good' deposits, in the sense that low resistivities and high metal concentrations are obtained.

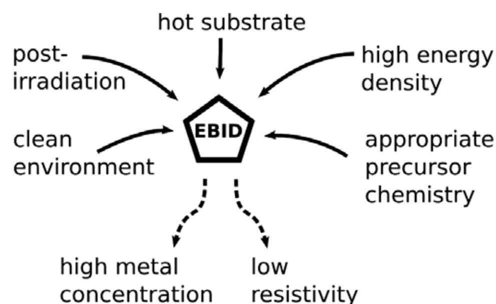

Figure 3. Schematic showing main paths to improving EBID depositions to obtain better purity materials.

One trend which has certainly emerged during the course of research for this review is the inconsistency of certain experiments within the community. Amusingly, van Dorp [58] referred to the state of the literature as a plethora of publications and results, and we find this is still true today. Very similar experiments often give contradictory results, and sometimes a single result is transformed into established

knowledge without having had confirmation from repeated experiments. Systematic studies with good reproducibility across different research groups are extremely rare. Of course research groups are naturally wary of spending precious time on repeating experiments which are deemed unlikely to yield good results: however, the present authors feel that the field as a whole would benefit from a more consistent body of knowledge.

Notwithstanding the issues of reproducibility, lack of accurate reporting and of standard experimental conditions, what can be seen to emerge from the existing body of research in EBID purification is that the possibility of creating pure material nanostructures is now potentially within reach. We can expect that within a few years selected metals will have known purification pathways to pure metal nanostructures, and we are still hopeful that, hand in hand with ongoing research into the fundamentals and understanding of the mechanism behind EBID through simulations such as [108], we will be able, within five to six years, to exert good control over the deposition process to achieve a nanostructure deposition according to user-desired specifications.

Acknowledgments

AB is grateful for funding from FEI Electron Optics. Despite the use of search engines and extensive efforts, the authors may still have missed relevant publications. We apologize if this is the case and ask to be informed.

References

[1] Feynmann R P 1959 *APS Mtg* California Institute of Technology
[2] Broers A 1988 *IBM J. Res. Dev.* **32** 49
[3] Grigorescu A E, van der Krogt M C, Hagen C W and Kruit P 2007 *J. Vac. Sci. Technol.* B **25** 1998–2003
[4] Barth J V, Costantini G and Kern K 2005 *Nature* **437** 671–9
[5] Randolph S J, Fowlkes J D and Rack P D 2006 *Crit. Rev. Solid State Mater. Sci.* **31** 55–89
[6] Silvis-Cividjian N, Hagen C W and Kruit P 2005 *J. Appl. Phys.* **98** 084905
[7] van Dorp W F, van Someren B, Hagen C W, Kruit P and Crozier P A 2005 *Nano Lett.* **5** 1303–7
[8] Molhave K, Madsen D N, Dohn S and Boggild P 2004 *Nanotechnology* **15** 1047–53
[9] Brintlinger T, Fuhrer M S, Melngailis J, Utke I, Bret T, Perentes A, Hoffmann P, Abourida M and Doppelt P 2005 *J. Vac. Sci. Technol.* B **23** 3174–7
[10] Koops H W P, Schoessler C, Kaya A and Weber M 1996 *J. Vac. Sci. Technol.* B **14** 4105–9
[11] Lau Y M, Chee P C, Thong J T L and Ng V 2002 *J. Vac. Sci. Technol.* A **20** 1295–302
[12] Broers A N, Molzen W W, Cuomo J J and Wittels D 1976 *J. Appl. Phys.* **29** 596–8
[13] von Platen K T K, Chlebek J, Weiss M, Reimer K, Oertel H and Brunger W H 1993 *J. Vac. Sci. Technol.* B **11** 2219–23
[14] Silvis-Cividjian N, Hagen C W, Leunissen L H A and Kruit P 2002 *Microelectron. Eng.* **61** 693–9
[15] Hagen C W, Silvis-Cividjian N and Kruit P 2005 *Scanning* **27** 90–1
[16] Fowlkes J D, Randolph S J and Rack P D 2005 *J. Vac. Sci. Technol.* B **23** 2825–31
[17] Utke I, Hoffmann P and Melngailis J 2008 *J. Vac. Sci. Technol.* B **26** 1197–276
[18] Shimojo M, Bysakh S, Mitsuishi K, Tanaka M, Song M and Furuya K 2005 *Appl. Surf. Sci.* **241** 56–60
[19] Graells S, Alcubilla R, Badeness G and Quidant R 2007 *Appl. Phys. Lett.* **91** 121112
[20] Utke I, Friedli V, Michler J, Bret T, Multone X and Hoffmann P 2006 *Appl. Phys. Lett.* **88** 031906
[21] Wang S, Sun Y-M and White J M 2005 *Appl. Surf. Sci.* **249** 110–4
[22] Luisier A, Utke I, Bret T, Cicoira F, Hauert R, Rhee S W, Doppelt P and Hoffmann P 2004 *J. Electrochem. Soc.* **151** C590–3
[23] Kakefuda Y, Yamashita Y, Mukai K and Yoshinobu J 2007 *Surf. Sci.* **601** 5108–11
[24] Takahashi T, Arakawa Y, Nishioka M and Ikoma T 1992 *Appl. Phys. Lett.* **60** 68–70
[25] Crozier P A, Tolle J, Kouvetakis J and Ritter C 2004 *Appl. Phys. Lett.* **84** 3441–3
[26] Ketharanathan S, Sharma R, Crozier P A and Drucker J 2006 *J. Vac. Sci. Technol.* B **24** 678–81
[27] Bret T, Utke I, Hoffmann P, Abourida M and Doppelt P 2006 *Microelectron. Eng.* **83** 1482–6
[28] George P M and Beauchamp J L 1980 *Thin Solid Films* **67** L25–8
[29] Weber M, Koops H W P, Rudolph M, Kretz J and Schmidt G 1995 *J. Vac. Sci. Technol.* B **13** 1364–8
[30] Perentes A, Sinicco G, Boero G, Dwir B and Hoffmann P 2007 *J. Vac. Sci. Technol.* B **25** 2228–32
[31] Scheuer V, Koops H and Tschudi T 1986 *Microelectron. Eng.* **5** 423–30
[32] Baker A G and Morris W C 1961 *Rev. Sci. Instrum.* **32** 458
[33] Spoddig D, Schindler K, Roediger P, Barzola-Quiquia J, Frtisch K, Mulders J and Esquinazi P 2007 *Nanotechnology* **18** 495202
[34] Gazzadi G C, Frabboni S and Menozzi C 2007 *Nanotechnology* **18** 445709
[35] Utke I, Dwir B, Leifer K, Cicoira F, Doppelt P, Hoffmann P and Kapon E 2000 *Microelectron. Eng.* **53** 261–4
[36] Zhang W, Shimojo M and Furuya K 2008 *J. Mater. Sci.* **43** 2069–71
[37] Oon C H, Khong S H, Boothroyd C B and Thong J T L 2006 *J. Appl. Phys.* **99** 064309
[38] Perentes A, Bret T, Utke I, Hoffmann P and Vaupel M 2006 *J. Vac. Sci. Technol.* B **24** 587–91
[39] Choi Y R, Rack P D, Frost B and Joy D C 2007 *Scanning* **29** 171–6
[40] Morimoto H, Kishimoto T, Takai M, Yura S, Hosono A, Okuda S, Lipp S, Frey L and Ryssel H 1996 *Japan. J. Appl. Phys.* **35** 6623–5
[41] Sellmair J, Edinger K and Koops H W P 2005 *J. Vac. Sci. Technol.* B **23** 781–5
[42] Ishibashi A, Funato K and Mori Y 1991 *J. Vac. Sci. Technol.* B **9** 169–72
[43] Hoffmann P, Utke I, Cicoira F, Dwir B, Leifer K, Kapon E and Doppelt P 2000 *Mater. Res. Soc. Symp. Proc.* **624** 171
[44] Fernandez-Pacheco A, de Teresa J M, Cordoba R and Ibarra M R 2009 *J. Phys. D: Appl. Phys.* **42** 055005
[45] Kunz R R and Mayer T M 1988 *J. Vac. Sci. Technol.* B **6** 1557–64
[46] Lukasczyk T, Schirmer M, Steinrueck H-P and Marbach H 2008 *Small* **4** 841–6
[47] Stark T J, Mayer T M, Griffis D P and Russell P E 1992 *J. Vac. Sci. Technol.* B **10** 2685–9
[48] Barry J D, Ervin M, Molstad J, Wickenden A, Brintlinger T, Hoffmann P and Melngailis J 2006 *J. Vac. Sci. Technol.* B **24** 3165–8
[49] Bret T, Utke I, Bachmann A and Hoffmann P 2003 *Appl. Phys. Lett.* **83** 4005–7

[50] Boszo F and Avouris P 1988 *Appl. Phys. Lett.* **53** 1095–7
[51] Funsten H O, Boring J W and Johnson R E 1992 *J. Appl. Phys.* **71** 1475–84
[52] Matsui S and Mori K 1986 *J. Vac. Sci. Technol.* B **4** 299–304
[53] Rotkina L, Oh S, Eckstein J N and Rotkin S V 2005 *Phys. Rev.* B **72** 233407
[54] Nam C Y, Tham D and Fischer J E 2005 *Nano Lett.* **5** 2029–33
[55] Luxmoore I J, Ross I M, Cullis A G, Fry P W, Orr J, Buckle P D and Jefferson J H 2007 *Thin Solid Films* **515** 6791–7
[56] Wnuk J D, Gorham J M, Rosenberg S G, van Dorp W F, Madey T E, Hagen C W and Fairbrother D H 2009 *J. Phys. Chem.* C **113** 2487–96
[57] Furuya K 2008 *Sci. Technol. Adv. Mater.* **9** 014110
[58] van Dorp W F and Hagen C W 2008 *J. Appl. Phys.* **104** 081301
[59] Matsui S, Kaito T, Ichi Fujita J, Komuro M, Kanda K and Haruyama Y 2000 *J. Vac. Sci. Technol.* B **18** 3181–4
[60] Mitsuishi K, Liu Z Q, Shimojo M, Han M and Furuya K 2005 *Ultramicroscopy* **103** 17–22
[61] Liu Z-Q, Mitsuishi K and Furuya K 2005 *Japan. J. Appl. Phys.* **44** 5659–63
[62] Liu Z-Q, Mitsuishi K and Furuya K 2006 *Microsc. Microanal.* **12** 1–4
[63] Utke I, Friedli V, Purrucker M and Michler J 2007 *J. Vac. Sci. Technol.* B **25** 2219–23
[64] Smith D A, Fowlkes J D and Rack P D 2007 *Nanotechnology* **18** 265308
[65] Lane C D and Orlando T M 2007 *Appl. Surf. Sci.* **253** 6646–56
[66] Nakano K, Horie T and Sakamoto H 1996 *Japan. J. Appl. Phys.* **35** 6570–3
[67] Randolph S J, Fowlkes J D and Rack P D 2005 *J. Appl. Phys.* **97** 124312
[68] Botman A, Mulders J J L, Weemaes R and Mentink S 2006 *Nanotechnology* **17** 3779–85
[69] Beaulieu D, Ding Y, Wang Z L and Lackey W J 2005 *J. Vac. Sci. Technol.* B **23** 2151–9
[70] Botman A, Hesselberth M and Mulders J J L 2008 *Microelectron. Eng.* **85** 1139–42
[71] Hoyle P C, Ogasawara M, Cleaver J R A and Ahmed H 1993 *Appl. Phys. Lett.* **62** 3043–5
[72] Hoyle P C, Cleaver J R A and Ahmed H 1994 *Appl. Phys. Lett.* **64** 1448–50
[73] Weber M, Rudolph M, Kretz J and Koops H W P 1995 *J. Vac. Sci. Technol.* B **13** 461–4
[74] Utke I, Bret T, Laub D, Buffat P, Scandella L and Hoffmann P 2004 *Microelectron. Eng.* **73** 553–8
[75] Utke I, Michler J, Gasser P, Santschi C, Laub D, Cantoni M, Buffat P A, Jiao C and Hoffmann P 2005 *Adv. Mater.* **7** 323–31
[76] Bret T 2005 Physico-chemical study of the focused electron beam induced deposition process *PhD Thesis* EPFL http://library.epfl.ch/theses/?nr=3321
[77] Langford R M, Wang T X and Ozkaya D 2007 *Microelectron. Eng.* **84** 784–8
[78] Plank H, Gspan C, Dienstleder M, Kothleitner G and Hofer F 2008 *Nanotechnology* **19** 485302
[79] Hiroshima H and Komuro M 1998 *Nanotechnology* **9** 108–12
[80] Utke I, Hoffmann P, Dwir B, Leifer K, Kapon E and Doppelt P 2000 *J. Vac. Sci. Technol.* B **18** 3168–71
[81] Miyazoe H, Kiriu S, Strauss S, Utke I, Michler J and Terashima K 2008 *Proc. FEBIP 2008* vol 1, pp 99–100
[82] Frabboni S, Gazzadi G C, Felisari L and Spessot A 2006 *Appl. Phys. Lett.* **88** 213116
[83] Egerton R F, Li P and Malac M 2004 *Micron* **35** 399–409
[84] Botman A, Hesselberth M and Mulders J J L 2008 *J. Vac. Sci. Technol.* B **26** 2464–7
[85] Xie G, Song M, Mitsuishi K and Furuya K 2005 *Physica* E **29** 564–9
[86] Takeguchi M, Shimojo M and Furuya K 2008 *Appl. Phys.* A **93** 439–42
[87] Hoyle P C, Cleaver J R A and Ahmed H 1996 *J. Vac. Sci. Technol.* B **14** 662–73
[88] Song M and Furuya K 2008 *Sci. Technol. Adv. Mater.* **9** 023002
[89] Toth M, Lobo C J, Hartigan G and Knowles W R 2007 *J. Appl. Phys.* **101** 054309
[90] Folch A, Servat J, Esteve J, Tejada J and Seco M 1996 *J. Vac. Sci. Technol.* B **14** 2609–14
[91] Matsui S and Ichihashi T 1988 *Appl. Phys. Lett.* **53** 842–4
[92] Cicoira F, Hoffmann P, Olsson C O A, Xanthopoulos N, Mathieu H J and Doppelt P 2005 *Appl. Surf. Sci.* **242** 107–13
[93] XEI Scientific, Inc. http://www.evactron.com/
[94] Berry G J, Cairns J A and Thomson J 1995 *Sensors Actuators* **51** 47–50
[95] Ochiai Y, Ichi Fujita J and Matsui S 1996 *J. Vac. Sci. Technol.* B **14** 3887–91
[96] Utke I, Friedli V, Amorosi S, Michler J and Hoffmann P 2006 *Microelectron. Eng.* **83** 1499–502
[97] Bret T, Utke I and Hoffmann P 2005 *Microelectron. Eng.* **78** 307–13
[98] Bret T, Utke I, Gaillard C and Hoffmann P 2004 *J. Vac. Sci. Technol.* B **22** 2504–10
[99] Mezhenny S, Lyubinetsky I, Choyke W J and Yates J T 1999 *J. Appl. Phys.* **85** 3368–73
[100] Thurier C and Doppelt P 2008 *Coord. Chem. Rev.* **252** 155–69
[101] Aaltonen T, Ritala M, Sajavaara T, Keinonen J and Leskela M 2003 *Chem. Mater.* **15** 1924–8
[102] Lee J M, Hwang C S, Cho H-J, Suk C-G and Kim H J 1998 *J. Electrochem. Soc.* **145** 1066–9
[103] Maya L, Riester L, Thundat T and Yust C S 1998 *J. Appl. Phys.* **84** 6382–6
[104] Okada Y, Shimomura H and Kawabe M 1993 *J. Appl. Phys.* **73** 7376–84
[105] Chiang T P, Sawin H H and Thompson C V 1997 *J. Vac. Sci. Technol.* A **15** 2677–86
[106] Basu J, Carter C B, Divakar R, Shenoy V B and Ravishankar N 2008 *Appl. Phys. Lett.* **93** 133104
[107] Friedli V and Utke I 2009 *J. Phys. D: Appl. Phys.* **42** 125305
[108] Smith D A, Fowlkes J D and Rack P D 2008 *Nanotechnology* **19** 415704
[109] Blauner P G, Butt Y, Ro J S, Thompson C V and Melngailis J 1989 *J. Vac. Sci. Technol.* B **7** 1816–8
[110] Kislov N A, Khodos I I, Ivanov E D and Barthel J 1996 *Scanning* **18** 114–8
[111] Chiang T P, Sawin H H and Thompson C V 1997 *J. Vac. Sci. Technol.* A **15** 3104–14
[112] Ratta A D D, Melngailis J and Thompson C V 1993 *J. Vac. Sci. Technol.* B **11** 2195–9
[113] Gannon T J, Gu G, Casey J D and Huynh C 2004 *J. Vac. Sci. Technol.* B **22** 3000–3
[114] Hochleitner G, Wanzenboeck H D and Bertagnolli E 2008 *J. Vac. Sci. Technol.* B **26** 939–44
[115] Shimojo M, Takeguchi M, Che R, Zhang W, Tanaka M, Mitsuishi K and Furuya K 2006 *Japan. J. Appl. Phys.* **45** 5509–12
[116] Takeguchi M, Shimojo M and Furuya K 2005 *Nanotechnology* **16** 1321–5
[117] Tanaka M, Chu F, Shimojo M, Takeguchi M, Mitsuishi K and Furuya K 2005 *Appl. Phys. Lett.* **86** 183104
[118] Tanaka M, Mitsuishi K, Takeguchi M, Shimojo M, Furuya K and Koguchi N 2007 *Japan. J. Appl. Phys.* **46** 6243–6
[119] Zhang W, Che R, Takeguchi M, Shimojo M and Furuya K 2006 *Surf. Interface Anal.* **38** 1527–9
[120] Tsukatani Y, Yamasaki N, Murakami K, Wakaya F and Takai M 2005 *Japan. J. Appl. Phys.* **44** 5683–6
[121] Gopal V, Radmilovic V R, Daraio C, Jin S, Yang P and Stach E A 2004 *Nano Lett.* **4** 2059–63

[122] Botman A and Mulders J J L 2008 private communication
[123] Liao Z-M, Xu J, Zhang X-Z and Yu D-P 2008 *Nanotechnology* **19** 305402
[124] Tao T, Ro J, Melgailis J, Xue Z and Kraesz H D 1990 *J. Vac. Sci. Technol.* B **8** 1826–9
[125] Ervin M H, Chang D, Nichols B, Wickenden A, Barry J and Melngailis J 2007 *J. Vac. Sci. Technol.* B **25** 2250–4
[126] Wang S, Sun Y M, Wang Q and White J M 2004 *J. Vac. Sci. Technol.* B **22** 1803–6
[127] Liu Z-Q, Mitsuishi K and Furuya K 2006 *Japan. J. Appl. Phys.* **45** 5548–51
[128] Koops H W P, Kaya A and Weber M 1995 *J. Vac. Sci. Technol.* B **13** 2400–3
[129] Zhang W, Shimojo M, Takeguchi M and Furuya K 2006 *J. Mater. Sci.* **41** 2577–80
[130] Bruk M A, Zhikharev E N, Grigoev E I, Spirin A V, Kalnov V A and Kardash I E 2005 *High Energy Chem.* **39** 65–8
[131] Kohlmann K T, Thiemann M and Brunger W H 1991 *Microelectron. Eng.* **13** 279–82
[132] Liu Z-Q, Mitsuishi K and Furuya K 2007 *Japan. J. Appl. Phys.* **46** 6254–7
[133] Klein K L, Randolph S J, Fowlkes J D, Allard L F, Meyer H M, Simpson M L and Rack P D 2008 *Nanotechnology* **19** 345705
[134] Li J, Toth M, Tileli V, Dunn K A, Lobo C J and Thiel B L 2008 *Appl. Phys. Lett.* **93** 023130
[135] Komuro M, Hiroshima H and Takechi A 1998 *Nanotechnology* **9** 104–7
[136] Miyazoe H, Sai M, Stauss S and Terashima K 2009 *J. Vac. Sci. Technol.* A **27** 9–12
[137] Prestigiacomo M, Bedu F, Jandard F, Tonneau D, Dellaporta H, Roussel L and Sudraud P 2005 *Appl. Phys. Lett.* **86** 192112
[138] Reguer A, Bedu F, Tonneau D, Dellaporta H, Prestigiacomo M, Houel A and Sudraud P 2008 *J. Vac. Sci. Technol.* B **26** 175–80
[139] Molhave K, Madsen D N, Rasmussen A M, Carlsson A, Appel C C, Brorson M, Jacobsen C J H and Boggild P 2003 *Nano Lett.* **3** 1499–503
[140] Folch A, Tejada J, Peters C H and Wrighton M S 1995 *Appl. Phys. Lett.* **66** 2080–2
[141] Shimojo M, Takeguchi M and Furuya K 2006 *Nanotechnology* **17** 3637–40
[142] Shimojo M, Takeguchi M, Mitsuishi K, Tanaka M and Furuya K 2007 *Japan. J. Appl. Phys.* **46** 6247–9
[143] Takeguchi M, Shimojo M and Furuya K 2007 *Japan. J. Appl. Phys.* **46** 6183–6
[144] Tseng A A 2007 *Nanofabrication: Fundamentals and Applications* (Singapore: World Scientific)
[145] Langford R M, Ozkaya D, Sheridan J and Chater R 2004 *Microsc. Microanal.* **10** 1122–3
[146] Wanzenboeck H D, Fischer M, Svagera R, Wernisch J and Bertagnolli E 2006 *J. Vac. Sci. Technol.* B **24** 2755–60
[147] Perentes A and Hoffmann P 2007 *J. Vac. Sci. Technol.* B **25** 2233–8
[148] Fischer M, Wanzenboeck H D, Gottsbachner J, Muller S, Brezna W, Schramboeck M and Bertagnolli E 2006 *Microelectron. Eng.* **83** 784–7
[149] Sato T, Mitsui M, Yamanaka J, Nakagawa K, Aoki Y, Sato S and Miyata C 2006 *Thin Solid Films* **508** 61–4
[150] Christy R W 1962 *J. Appl. Phys.* **33** 1884–8
[151] Kim S H and Somorjai G A 2002 *J. Phys. Chem.* B **106** 1386–91
[152] Kakefuda Y, Yamashita Y, Mukai K and Yoshinobu J 2006 *Rev. Sci. Instrum.* **77** 053702
[153] Hiroshima H, Suzuki N, Ogawa N and Komuro M 1999 *Japan. J. Appl. Phys.* **38** 7135–9
[154] Jackman R B and Foord J S 1986 *Appl. Phys. Lett.* **49** 196–8
[155] Lassiter M G, Liang T and Rack P D 2008 *J. Vac. Sci. Technol.* B **26** 963–7
[156] Bhuvana T and Kulkarni G U 2008 *ACS Nano* **2** 457–62
[157] Houlding V H, Clements N S and Beeson K W 1987 *J. Appl. Phys.* **62** 1070–3
[158] Rand M J 1973 *J. Electrochem. Soc.: Solid State Sci. Technol.* **120** 686–93